Eur. Phys. J. C (2010) 69: 347–360
DOI 10.1140/epjc/s10052-010-1423-2

THE EUROPEAN PHYSICAL JOURNAL C

Regular Article - Experimental Physics

Measurement of beauty production in DIS and $F_2^{b\bar{b}}$ extraction at ZEUS

The ZEUS Collaboration

H. Abramowicz[44,ae], I. Abt[34], L. Adamczyk[13], M. Adamus[53], R. Aggarwal[7], S. Antonelli[4], P. Antonioli[3], A. Antonov[32], M. Arneodo[49], V. Aushev[26,z], Y. Aushev[26,z], O. Bachynska[15], A. Bamberger[19], A.N. Barakbaev[25], G. Barbagli[17], G. Bari[3], F. Barreiro[29], D. Bartsch[5], M. Basile[4], O. Behnke[15], J. Behr[15], U. Behrens[15], L. Bellagamba[3], A. Bertolin[38], S. Bhadra[56], M. Bindi[4], C. Blohm[15], T. Bołd[13], E.G. Boos[25], M. Borodin[26], K. Borras[15], D. Boscherini[3], D. Bot[15], S.K. Boutle[51], I. Brock[5], E. Brownson[55], R. Brugnera[39], N. Brümmer[36], A. Bruni[3], G. Bruni[3], B. Brzozowska[52], P.J. Bussey[20], J.M. Butterworth[51], B. Bylsma[36], A. Caldwell[34], M. Capua[8], R. Carlin[39], C.D. Catterall[56], S. Chekanov[1], J. Chwastowski[12,g], J. Ciborowski[52,aj], R. Ciesielski[15,i], L. Cifarelli[4], F. Cindolo[3], A. Contin[4], A.M. Cooper-Sarkar[37], N. Coppola[15,j], M. Corradi[3], F. Corriveau[30], M. Costa[48], G. D'Agostini[42], F. Dal Corso[38], J. de Favereau[28], J. del Peso[29], R.K. Dementiev[33], S. De Pasquale[4,c], M. Derrick[1], R.C.E. Devenish[37], D. Dobur[19], B.A. Dolgoshein[32], A.T. Doyle[20], V. Drugakov[16], L.S. Durkin[36], S. Dusini[38], Y. Eisenberg[54], P.F. Ermolov[33,an], A. Eskreys[12], S. Fang[15], S. Fazio[8], J. Ferrando[37], M.I. Ferrero[48], J. Figiel[12], M. Forrest[20], B. Foster[37], S. Fourletov[50,ai], G. Gach[13], A. Galas[12], E. Gallo[17], A. Garfagnini[39], A. Geiser[15], I. Gialas[21,v], L.K. Gladilin[33], D. Gladkov[32], C. Glasman[29], O. Gogota[26], Yu.A. Golubkov[33], P. Göttlicher[15,k], I. Grabowska-Bołd[13], J. Grebenyuk[15], I. Gregor[15], G. Grigorescu[35], G. Grzelak[52], C. Gwenlan[37,ab], T. Haas[15,a], W. Hain[15], R. Hamatsu[47], J.C. Hart[43], H. Hartmann[5], G. Hartner[56], E. Hilger[5], D. Hochman[54], U. Holm[22], R. Hori[46], K. Horton[37,ac], A. Hüttmann[15], G. Iacobucci[3], Z.A. Ibrahim[10], Y. Iga[41], R. Ingbir[44], M. Ishitsuka[45], H.-P. Jakob[5], F. Januschek[15], M. Jimenez[29], T.W. Jones[51], M. Jüngst[5], I. Kadenko[26], B. Kahle[15], B. Kamaluddin[10,an], S. Kananov[44], T. Kanno[45], U. Karshon[54], F. Karstens[19], I.I. Katkov[15,l], M. Kaur[7], P. Kaur[7,e], A. Keramidas[35], L.A. Khein[33], J.Y. Kim[9], D. Kisielewska[13], S. Kitamura[47,af], R. Klanner[22], U. Klein[15,m], E. Koffeman[35], D. Kollar[34], P. Kooijman[35], Ie. Korol[26], I.A. Korzhavina[33], A. Kotański[14,h], U. Kötz[15], H. Kowalski[15], P. Kulinski[52], O. Kuprash[26], M. Kuze[45], V.A. Kuzmin[33], A. Lee[36], B.B. Levchenko[33,aa], A. Levy[44], V. Libov[15], S. Limentani[39], T.Y. Ling[36], M. Lisovyi[15], E. Lobodzinska[15], W. Lohmann[16], B. Löhr[15], E. Lohrmann[22], J.H. Loizides[51], K.R. Long[23], A. Longhin[38], D. Lontkovskyi[26], O.Yu. Lukina[33], P. Łużniak[52,ak], J. Maeda[45], S. Magill[1], I. Makarenko[26], J. Malka[52,ak], R. Mankel[15,n], A. Margotti[3], G. Marini[42], J.F. Martin[50], A. Mastroberardino[8], T. Matsumoto[24,w], M.C.K. Mattingly[2], I.-A. Melzer-Pellmann[15], S. Miglioranzi[15,o], F. Mohamad Idris[10], V. Monaco[48], A. Montanari[15], J.D. Morris[6,d], B. Musgrave[1], K. Nagano[24], T. Namsoo[15,p], R. Nania[3], D. Nicholass[1,b], A. Nigro[42], Y. Ning[11], U. Noor[56], D. Notz[15], R.J. Nowak[52], A.E. Nuncio-Quiroz[5], B.Y. Oh[40], N. Okazaki[46], K. Oliver[37], K. Olkiewicz[12], Yu. Onishchuk[26], O. Ota[47,ag], K. Papageorgiu[21], A. Parenti[15], E. Paul[5], J.M. Pawlak[52], B. Pawlik[12], P.G. Pelfer[18], A. Pellegrino[35], W. Perlanski[52,ak], H. Perrey[22], K. Piotrzkowski[28], P. Plucinski[53,al], N.S. Pokrovskiy[25], A. Polini[3], A.S. Proskuryakov[33], M. Przybycień[13], A. Raval[15], D.D. Reeder[55], B. Reisert[34], Z. Ren[11], J. Repond[1], Y.D. Ri[47,ah], A. Robertson[37], P. Roloff[15], E. Ron[29], I. Rubinsky[15], M. Ruspa[49], R. Sacchi[48], A. Salii[26], U. Samson[5], G. Sartorelli[4], A.A. Savin[55], D.H. Saxon[20], M. Schioppa[8], S. Schlenstedt[16], P. Schleper[22], W.B. Schmidke[34], U. Schneekloth[15], V. Schönberg[5], T. Schörner-Sadenius[22], J. Schwartz[30], F. Sciulli[11], L.M. Shcheglova[33], R. Shehzadi[5], S. Shimizu[46,o], I. Singh[7,e], I.O. Skillicorn[20], W. Słomiński[14], W.H. Smith[55], V. Sola[48], A. Solano[48], D. Son[27], V. Sosnovtsev[32], A. Spiridonov[15,q], H. Stadie[22], L. Stanco[38], A. Stern[44], T.P. Stewart[50], A. Stifutkin[32], P. Stopa[12], S. Suchkov[32], G. Susinno[8], L. Suszycki[13], J. Sztuk[22], D. Szuba[15,r], J. Szuba[15,s], A.D. Tapper[23], E. Tassi[8,f], J. Terrón[29], T. Theedt[15], H. Tiecke[35], K. Tokushuku[24,x], O. Tomalak[26], J. Tomaszewska[15,t], T. Tsurugai[31], M. Turcato[22], T. Tymieniecka[53,am], C. Uribe-Estrada[29], M. Vázquez[35,o], A. Verbytskyi[15], V. Viazlo[26], N.N. Vlasov[19,u], O. Volynets[26], R. Walczak[37], W.A.T. Wan Abdullah[10], J.J. Whitmore[40,ad], J. Whyte[56], L. Wiggers[35], M. Wing[51], M. Wlasenko[5], G. Wolf[15], H. Wolfe[55], K. Wrona[15], A.G. Yagües-Molina[15], S. Yamada[24], Y. Yamazaki[24,y], R. Yoshida[1], C. Youngman[15], A.F. Żarnecki[52], L. Zawiejski[12], O. Zenaiev[26], W. Zeuner[15,o], B.O. Zhautykov[25], N. Zhmak[26,z], C. Zhou[30], A. Zichichi[4], M. Zolko[26], D.S. Zotkin[33], Z. Zulkapli[10]

[1] Argonne National Laboratory, Argonne, IL 60439-4815, USA[ao]
[2] Andrews University, Berrien Springs, MI 49104-0380, USA
[3] INFN Bologna, Bologna, Italy[ap]
[4] University and INFN Bologna, Bologna, Italy[ap]
[5] Physikalisches Institut der Universität Bonn, Bonn, Germany[aq]
[6] H.H. Wills Physics Laboratory, University of Bristol, Bristol, UK[ar]
[7] Panjab University, Department of Physics, Chandigarh, India
[8] Calabria University, Physics Department and INFN, Cosenza, Italy[ap]
[9] Institute for Universe and Elementary Particles, Chonnam National University, Kwangju, South Korea
[10] Jabatan Fizik, Universiti Malaya, 50603 Kuala Lumpur, Malaysia[as]
[11] Nevis Laboratories, Columbia University, Irvington on Hudson, NY 10027, USA[at]
[12] The Henryk Niewodniczanski Institute of Nuclear Physics, Polish Academy of Sciences, Cracow, Poland[au]
[13] Faculty of Physics and Applied Computer Science, AGH-University of Science and Technology, Cracow, Poland[av]
[14] Department of Physics, Jagellonian University, Cracow, Poland
[15] Deutsches Elektronen-Synchrotron DESY, Hamburg, Germany
[16] Deutsches Elektronen-Synchrotron DESY, Zeuthen, Germany
[17] INFN Florence, Florence, Italy[ap]
[18] University and INFN Florence, Florence, Italy[ap]
[19] Fakultät für Physik der Universität Freiburg i.Br., Freiburg i.Br., Germany[aq]
[20] Department of Physics and Astronomy, University of Glasgow, Glasgow, UK[ar]
[21] Department of Engineering in Management and Finance, Univ. of the Aegean, Chios, Greece
[22] Hamburg University, Institute of Exp. Physics, Hamburg, Germany[aq]
[23] Imperial College London, High Energy Nuclear Physics Group, London, UK[ar]
[24] Institute of Particle and Nuclear Studies, KEK, Tsukuba, Japan[aw]
[25] Institute of Physics and Technology of Ministry of Education and Science of Kazakhstan, Almaty, Kazakhstan
[26] Institute for Nuclear Research, National Academy of Sciences, and Kiev National University, Kiev, Ukraine
[27] Kyungpook National University, Center for High Energy Physics, Daegu, South Korea[ax]
[28] Institut de Physique Nucléaire, Université Catholique de Louvain, Louvain-la-Neuve, Belgium[ay]
[29] Departamento de Física Teórica, Universidad Autónoma de Madrid, Madrid, Spain[az]
[30] Department of Physics, McGill University, Montréal, Québec, Canada H3A 2T8[ba]
[31] Meiji Gakuin University, Faculty of General Education, Yokohama, Japan[aw]
[32] Moscow Engineering Physics Institute, Moscow, Russia[bb]
[33] Moscow State University, Institute of Nuclear Physics, Moscow, Russia[bc]
[34] Max-Planck-Institut für Physik, München, Germany
[35] NIKHEF and University of Amsterdam, Amsterdam, Netherlands[bd]
[36] Physics Department, Ohio State University, Columbus, OH 43210, USA[ao]
[37] Department of Physics, University of Oxford, Oxford, UK[ar]
[38] INFN Padova, Padova, Italy[ap]
[39] Dipartimento di Fisica dell' Università and INFN, Padova, Italy[ap]
[40] Department of Physics, Pennsylvania State University, University Park, PA 16802, USA[at]
[41] Polytechnic University, Sagamihara, Japan[aw]
[42] Dipartimento di Fisica, Università 'La Sapienza' and INFN, Rome, Italy[ap]
[43] Rutherford Appleton Laboratory, Chilton, Didcot, Oxon, UK[ar]
[44] Raymond and Beverly Sackler Faculty of Exact Sciences, School of Physics, Tel Aviv University, Tel Aviv, Israel[be]
[45] Department of Physics, Tokyo Institute of Technology, Tokyo, Japan[aw]
[46] Department of Physics, University of Tokyo, Tokyo, Japan[aw]
[47] Tokyo Metropolitan University, Department of Physics, Tokyo, Japan[aw]
[48] Università di Torino and INFN, Torino, Italy[ap]
[49] Università del Piemonte Orientale, Novara, and INFN, Torino, Italy[ap]
[50] Department of Physics, University of Toronto, Toronto, Ontario, Canada M5S 1A7[ba]
[51] Physics and Astronomy Department, University College London, London, UK[ar]
[52] Warsaw University, Institute of Experimental Physics, Warsaw, Poland
[53] Institute for Nuclear Studies, Warsaw, Poland
[54] Department of Particle Physics, Weizmann Institute, Rehovot, Israel[bf]
[55] Department of Physics, University of Wisconsin, Madison, WI 53706, USA[ao]
[56] Department of Physics, York University, Ontario, Canada M3J 1P3[ba]

Received: 1 June 2010 / Revised: 3 August 2010 / Published online: 2 September 2010

[a] e-mail: tobias.haas@desy.de
[b] Also affiliated with University College London, UK.
[c] Now at University of Salerno, Italy.
[d] Now at Queen Mary University of London, UK.

Abstract Beauty production in deep inelastic scattering with events in which a muon and a jet are observed in the final state has been measured with the ZEUS detector at HERA using an integrated luminosity of 114 pb^{-1}. The fraction of events with beauty quarks in the data was determined using the distribution of the transverse momentum of the muon relative to the jet. The cross section for beauty production was measured in the kinematic range of photon virtuality, $Q^2 > 2$ GeV^2, and inelasticity, $0.05 < y < 0.7$, with the requirement of a muon and a jet. Total and differential cross sections are presented and compared to QCD predictions. The beauty contribution to the structure function F_2 was extracted and is compared to theoretical predictions.

1 Introduction

The production of beauty quarks in ep collisions at HERA provides a stringent test of perturbative Quantum Chromodynamics (QCD), since the large b-quark mass

[e] Also working at Max Planck Institute, Munich, Germany.

[f] Also Senior Alexander von Humboldt Research Fellow at Hamburg University, Institute of Experimental Physics, Hamburg, Germany.

[g] Also at Cracow University of Technology, Faculty of Physics, Mathemathics and Applied Computer Science, Poland.

[h] Supported by the research grant No. 1 P03B 04529 (2005–2008).

[i] Now at Rockefeller University, New York, NY 10065, USA.

[j] Now at DESY group FS-CFEL-1.

[k] Now at DESY group FEB, Hamburg, Germany.

[l] Also at Moscow State University, Russia.

[m] Now at University of Liverpool, UK.

[n] On leave of absence at CERN, Geneva, Switzerland.

[o] Now at CERN, Geneva, Switzerland.

[p] Now at Goldman Sachs, London, UK.

[q] Also at Institute of Theoretical and Experimental Physics, Moscow, Russia.

[r] Also at INP, Cracow, Poland.

[s] Also at FPACS, AGH-UST, Cracow, Poland.

[t] Partially supported by Warsaw University, Poland.

[u] Partially supported by Moscow State University, Russia.

[v] Also affiliated with DESY, Germany.

[w] Now at Japan Synchrotron Radiation Research Institute (JASRI), Hyogo, Japan.

[x] Also at University of Tokyo, Japan.

[y] Now at Kobe University, Japan.

[z] Supported by DESY, Germany.

[aa] Partially supported by Russian Foundation for Basic Research grant No. 05-02-39028-NSFC-a.

[ab] STFC Advanced Fellow.

[ac] Née Korcsak-Gorzo.

[ad] This material was based on work supported by the National Science Foundation, while working at the Foundation.

[ae] Also at Max Planck Institute, Munich, Germany, Alexander von Humboldt Research Award.

[af] Now at Nihon Institute of Medical Science, Japan.

[ag] Now at SunMelx Co. Ltd., Tokyo, Japan.

[ah] Now at Osaka University, Osaka, Japan.

[ai] Now at University of Bonn, Germany.

[aj] Also at Łódź University, Poland.

[ak] Member of Łódź University, Poland.

[al] Now at Lund University, Lund, Sweden.

[am] Also at University of Podlasie, Siedlce, Poland.

[an] Deceased.

[ao] Supported by the US Department of Energy.

[ap] Supported by the Italian National Institute for Nuclear Physics (INFN).

[aq] Supported by the German Federal Ministry for Education and Research (BMBF), under contract Nos. 05 HZ6PDA, 05 HZ6GUA, 05 HZ6VFA and 05 HZ4KHA.

[ar] Supported by the Science and Technology Facilities Council, UK.

[as] Supported by an FRGS grant from the Malaysian government.

[at] Supported by the US National Science Foundation. Any opinion, findings and conclusions or recommendations expressed in this material are those of the authors and do not necessarily reflect the views of the National Science Foundation.

[au] Supported by the Polish Ministry of Science and Higher Education as a scientific project No. DPN/N188/DESY/2009.

[av] Supported by the Polish Ministry of Science and Higher Education as a scientific project (2009–2010).

[aw] Supported by the Japanese Ministry of Education, Culture, Sports, Science and Technology (MEXT) and its grants for Scientific Research.

[ax] Supported by the Korean Ministry of Education and Korea Science and Engineering Foundation.

[ay] Supported by FNRS and its associated funds (IISN and FRIA) and by an Inter-University Attraction Poles Programme subsidised by the Belgian Federal Science Policy Office.

[az] Supported by the Spanish Ministry of Education and Science through funds provided by CICYT.

[ba] Supported by the Natural Sciences and Engineering Research Council of Canada (NSERC).

[bb] Partially supported by the German Federal Ministry for Education and Research (BMBF).

[bc] Supported by RF Presidential grant N 1456.2008.2 for the leading scientific schools and by the Russian Ministry of Education and Science through its grant for Scientific Research on High Energy Physics.

[bd] Supported by the Netherlands Foundation for Research on Matter (FOM).

[be] Supported by the Israel Science Foundation.

[bf] Supported in part by the MINERVA Gesellschaft für Forschung GmbH, the Israel Science Foundation (grant No. 293/02-11.2) and the US-Israel Binational Science Foundation.

($m_b \approx 5$ GeV) provides a hard scale that should ensure reliable predictions in all regions of phase space, including the kinematic threshold. Especially in this region, with b-quark transverse momenta comparable to or less than the b-quark mass, next-to-leading-order (NLO) QCD calculations based on the mechanism of dynamical generation of the (massive) b quarks [1–6] are expected to provide accurate predictions.

The cross section for beauty production has previously been measured in ep collisions [7–20], as well as in $p\overline{p}$ collisions at the S$p\overline{p}$S [21–24] and Tevatron [25–39] colliders, in $\gamma\gamma$ interactions at LEP [40–42], and in fixed-target πN [43, 44] and pN [45–47] experiments. Most results, including recent results from the Tevatron, are in good agreement with QCD predictions. Some of the LEP results [40], however, deviate from the predictions.

This paper reports on a ZEUS measurement of beauty production in deep inelastic scattering (DIS) extending the kinematic region of previous ZEUS measurements [16, 17]. The class of events investigated is

$$ep \to eb\overline{b}X \to e \text{ jet } \mu X',$$

in which at least one jet and one muon are found in the final state. A data set partially overlapping with that of the first ZEUS measurement [16] was used. Looser cuts on muons and jets were applied. For muon identification, an extended combination of detector components was used. This resulted in a better detection efficiency than obtained in the previous analysis and allowed the threshold of the muon transverse momentum to be lowered. This is important for the extraction of the beauty contribution to the proton structure function, $F_2^{b\overline{b}}$, for which an extrapolation to the full phase space has to be performed. Such an extraction was already performed by the ZEUS collaboration [17] using an independent data set covering the kinematic range $Q^2 > 20$ GeV^2. In the present analysis, the kinematic range of the measurement was extended to $Q^2 > 2$ GeV^2. A comparison to the results obtained by the H1 collaboration [18–20], using an inclusive impact parameter technique, is also presented in this paper.

Due to the large b-quark mass, muons from semi-leptonic b decays usually have high values of p_T^{rel}, the transverse momentum of the muon relative to the axis of the jet with which they are associated. For muons from charm decays, from K and π decays, and in events where a hadron is misidentified as a muon, the p_T^{rel} values are typically lower. Therefore, the fraction of events from b decays in the data sample can be extracted by fitting the p_T^{rel} distribution of the data using Monte Carlo (MC) predictions for the processes producing beauty, charm and light quarks.

In this analysis, the visible cross section, $\sigma_{b\bar{b}}$, and differential cross sections as a function of Q^2, the transverse momentum of the muon, p_T^{μ}, and its pseudorapidity,[1] η^{μ}, as well as the transverse momentum of the jet, p_T^{jet}, and its pseudorapidity, η^{jet}, were measured. They are compared to leading-order (LO) plus parton-shower (PS) MC predictions and NLO QCD calculations. The beauty contribution to the proton structure-function F_2 is extracted as a function of Q^2 and the Bjorken scaling variable, x, and compared to theoretical predictions.

2 Experimental set-up

The data sample used corresponds to an integrated luminosity $\mathcal{L} = 114.1 \pm 2.3\,\text{pb}^{-1}$, collected by the ZEUS detector in the years 1996–2000. During the 1996–1997 data taking, HERA provided collisions between an electron[2] beam of $E_e = 27.5$ GeV and a proton beam of $E_p = 820$ GeV, corresponding to a centre-of-mass energy $\sqrt{s} = 300$ GeV ($\mathcal{L}_{300} = 38.0 \pm 0.6$ pb^{-1}). In the years 1998–2000, the proton-beam energy was $E_p = 920$ GeV, corresponding to $\sqrt{s} = 318$ GeV ($\mathcal{L}_{318} = 76.1 \pm 1.7$ pb^{-1}).

A detailed description of the ZEUS detector can be found elsewhere [48]. A brief outline of the components that are most relevant for this analysis is given below. Charged particles were tracked in the central tracking detector (CTD) [49–51], which operated in a magnetic field of 1.43 T provided by a thin superconducting coil. The CTD consisted of 72 cylindrical drift chamber layers, organised in 9 superlayers covering the polar-angle region $15° < \theta < 164°$. The transverse-momentum resolution for full-length tracks is $\sigma(p_T)/p_T = 0.0058 p_T \oplus 0.0065 \oplus 0.0014/p_T$, with p_T in GeV.

The high-resolution uranium–scintillator calorimeter (CAL) [52–55] consisted of three parts: the forward (FCAL), the barrel (BCAL) and the rear (RCAL) calorimeters. Each part was subdivided transversely into towers and longitudinally into one electromagnetic section and either one (in RCAL) or two (in BCAL and FCAL) hadronic sections. The CAL energy resolutions, as measured under test-beam conditions, are $\sigma(E)/E = 0.18/\sqrt{E}$ for electrons and $\sigma(E)/E = 0.35/\sqrt{E}$ for hadrons, with E in GeV.

The muon system consisted of barrel, rear (B/RMUON) [56] and forward (FMUON) [48] tracking detectors. The

[1] The pseudorapidity is defined as $\eta = -\ln(\tan\frac{\theta}{2})$, where the polar angle, θ, is measured with respect to the Z axis. The ZEUS coordinate system is a right-handed Cartesian system, with the Z axis pointing in the proton beam direction, referred to as the "forward direction", and the X axis pointing towards the centre of HERA. The coordinate origin is at the nominal interaction point.

[2] Electrons and positrons are not distinguished in this paper and are both referred to as electrons.

B/RMUON consisted of limited-streamer (LS) tube chambers placed behind the BCAL (RCAL), inside and outside the magnetised iron yoke surrounding the CAL. The barrel and rear muon chambers covered polar angles from 34° to 135° and from 135° to 171°, respectively. The FMUON consisted of six planes of LS tubes and four planes of drift chambers covering the angular region from 5° to 32°. The muon system exploited the magnetic field of the iron yoke and, in the forward direction, of two iron toroids magnetised to 1.6 T to provide an independent measurement of the muon momentum.

Muons were also detected by the sampling Backing Calorimeter (BAC) [57]. This detector consisted of 5200 proportional drift chambers which were typically 5 m long and had a wire spacing of 1 cm. The chambers were inserted into the magnetised iron yoke (barrel and two endcaps) covering the CAL. The BAC was equipped with analogue (for energy measurement) and digital (for muon tracking) readouts. The digital information from the hit wires allowed the reconstruction of muon trajectories in two dimensions (XY in barrel, YZ in endcaps) with an accuracy of a few mm.

The luminosity was measured from the rate of the bremsstrahlung process $ep \to e\gamma p$. The resulting small-angle photons were measured by the luminosity monitor [58], a lead-scintillator calorimeter placed in the HERA tunnel at $Z = -107$ m.

3 Event selection and reconstruction

3.1 Trigger selection

Events containing either a scattered electron, a muon, two jets, or charmed hadrons were selected online by means of a three-level trigger system [48, 59] through a combination of four different trigger chains as explained elsewhere [15]. The average trigger efficiency for events within the chosen kinematic region with a jet and with a reconstructed muon from b-quark decay was $(93 \pm 2)\%$. For events with $Q^2 > 20\ \mathrm{GeV}^2$, the inclusive DIS triggers yielded an efficiency of almost 100%. For the lowest Q^2 values, $2 < Q^2 < 4\ \mathrm{GeV}^2$, the efficiency of the combined trigger chains was 73%.

3.2 General event selection

Offline, the event vertex was required to be reconstructed within $|Z| < 50$ cm around the interaction point. A well-reconstructed scattered electron with an impact point on the surface of the RCAL outside a region of ± 12 cm in X and ± 6 cm in Y around the beampipe and

$$E_e > 10\ \mathrm{GeV},$$

$$Q_e^2 > 2\ \mathrm{GeV}^2$$

was required, where the estimator of Q^2, Q_e^2, was reconstructed using the energy, E_e, and the angle of the scattered electron.

In order to reject events from photoproduction, $Q^2 < 1\ \mathrm{GeV}^2$, the following cuts were applied:

$$y_{\mathrm{JB}} > 0.05,$$

$$y_e < 0.7,$$

$$40 < E - p_Z < 65\ \mathrm{GeV},$$

where y_{JB} and y_e are estimators for the inelasticity, y, of the event. For small values of y, the Jacquet-Blondel estimator $y_{\mathrm{JB}} = (E - p_Z)/(2E_e)$ [60] was used, where $E - p_Z = \sum_i E^i - p_Z^i$ and the sum runs over all energy-flow objects (EFOs) [61]. EFOs combine the information from calorimetry and tracking, corrected for energy loss in dead material and for the presence of reconstructed muons.

The large mass of a $b\bar{b}$ pair, at least ≈ 10 GeV, usually leads to a significant amount of energy deposited in the central parts of the detector. To reduce backgrounds from light-flavour events and charm, a cut

$$E_T > 8\ \mathrm{GeV}$$

was applied, with

$$E_T = E_T^{\mathrm{cal}} - E_{T\,|10^\circ}^{\mathrm{cal}} - E_T^e,$$

where E_T^{cal} is the transverse energy deposited in the CAL, $E_{T\,|10^\circ}^{\mathrm{cal}}$ is the transverse energy in a cone of 10° around the forward beam pipe and E_T^e is the transverse energy of the scattered electron. The b and $\bar{b}$ quarks also fragment and decay into a large number of particles. Therefore events with a low number of observed tracks, N_{Tracks}, were rejected by requiring

$$N_{\mathrm{Tracks}} \geq 8.$$

3.3 Jet identification and selection

Hadronic final-state objects were reconstructed from EFOs, which were clustered into jets using the k_T cluster algorithm KTCLUS [62] in its massive mode with the E_T recombination scheme. The identified scattered electron was removed [63] before the clustering procedure, while reconstructed muons were included. Events were selected if they contained at least one jet with transverse energy, E_T^{jet}, of

$$E_T^{\mathrm{jet}} = p_T^{\mathrm{jet}} \frac{E^{\mathrm{jet}}}{p^{\mathrm{jet}}} > 5\ \mathrm{GeV},$$

where $E^{\rm jet}$, $p^{\rm jet}$ and $p_T^{\rm jet}$ are the jet energy, momentum and transverse momentum, and within the jet pseudorapidity ($\eta^{\rm jet}$) acceptance,

$$-2.0 < \eta^{\rm jet} < 2.5.$$

3.4 Muon identification and selection

Muons were selected offline if they satisfied at least one of the following criteria:

- a muon track was found in the inner B/RMUON chambers. A match in position and angle to a CTD track was required. In the bottom region, where no inner chambers are present, the outer chambers were used instead. For muons with hits in both inner and outer chambers, momentum consistency was required;
- a muon track was found in the FMUON chambers. Within the CTD acceptance, a match in position and angle to a CTD track was required and the momentum was obtained from a combined fit to the CTD and FMUON information. Outside the CTD acceptance, candidates well measured in FMUON only and fitted to the primary vertex were accepted;
- a muon track or localised energy deposit was found in the BAC, and matched to a CTD track, from which the muon momentum was obtained. In the forward region of the detector, an energy deposit in the calorimeter consistent with the passing of a minimum-ionising particle was required in addition in order to reduce background related to the proton beam or to the punch through of high-energy hadrons.

Most muons were within the geometric acceptance of more than one of these algorithms. The overall efficiency was about 80% for muons with momenta above 2–5 GeV, depending on the muon pseudorapidity, η^{μ}.

In the barrel region, the requirement that the muons reach at least the inner muon chambers implies a muon transverse momentum, p_T^{μ}, of about 1.5 GeV or more. In order to have approximately uniform pseudorapidity acceptance, a cut

$$p_T^{\mu} > 1.5 \text{ GeV}$$

was therefore applied to all muons. The coverage of the tracking and muon systems resulted in an implicit upper cut-off $\eta^{\mu} \lesssim 2.5$. The expected signal muon distribution suggested the explicit cut

$$\eta^{\mu} > -1.6.$$

A muon was associated with a jet if it was located within a cone of $\Delta R = \sqrt{\Delta\phi^2 + \Delta\eta^2} < 0.7$ around the jet axis, where $\Delta\phi$ and $\Delta\eta$ are the distances between the muon and the jet in azimuth angle and pseudorapidity, respectively. At least one muon associated with a jet was required.

After all selection cuts, the final data sample contained 19698 events. In each event, only the muon candidate with the highest p_T^{μ} was considered.

4 Monte Carlo simulation

To evaluate the detector acceptance and to provide the signal and background distributions, MC samples of beauty, charm, and light flavours (LF) were generated, corresponding to 17, three, and about one times the integrated luminosity of the data, respectively. The beauty and charm samples were generated using the RAPGAP 3 MC program [64] in the massive mode ($m_c = 1.5$ GeV, $m_b = 4.75$ GeV), interfaced to HERACLES 4.6.1 [65] in order to incorporate first-order electroweak corrections. In RAPGAP, LO matrix elements are combined with higher-order QCD radiation simulated in the leading-logarithmic approximation. The hadronisation is simulated using the Lund string model as implemented in JETSET [66]. The lepton energy spectrum from charm decays was reweighted to agree with CLEO data [67]. The lepton spectrum from beauty decays was found to be in good agreement [63] with that determined from e^+e^- data. An inclusive MC sample containing all flavours was generated in the massless mode using ARIADNE [68]. The subset containing only LF events was used for the background simulation, while the full sample was used for systematic studies.

The generated events were passed through a full simulation of the ZEUS detector based on GEANT 3.13 [69]. They were subjected to the same trigger requirements and processed by the same reconstruction programs as the data.

Imperfections of the simulation of the muon range in dense materials as well as of the efficiency of the muon detectors were corrected using an independent data set of isolated muons from J/ψ and Bethe-Heitler events [70]. Tabulated as a function of p_T^{μ} and η^{μ}, these corrections were applied to MC events on an event-by-event basis.

Figure 1 shows the comparison of the MC simulation to the data for a selection of variables of the measured muon and the associated jet. The MC agrees reasonably well with the measured distributions. This demonstrates that the MC can be reliably used to calculate the detector-acceptance corrections.

5 NLO calculations

Next-to-leading-order QCD predictions for the visible cross sections were obtained in the fixed-flavour-number scheme (FFNS) using HVQDIS [6]. The b-quark mass was set to $m_b = 4.75$ GeV and the renormalisation, μ_R, and factorisation, μ_F, scales to $\mu_R = \mu_F = \frac{1}{2}\sqrt{Q^2 + p_T^2 + m_b^2}$, where p_T is the average transverse momentum of the two b quarks

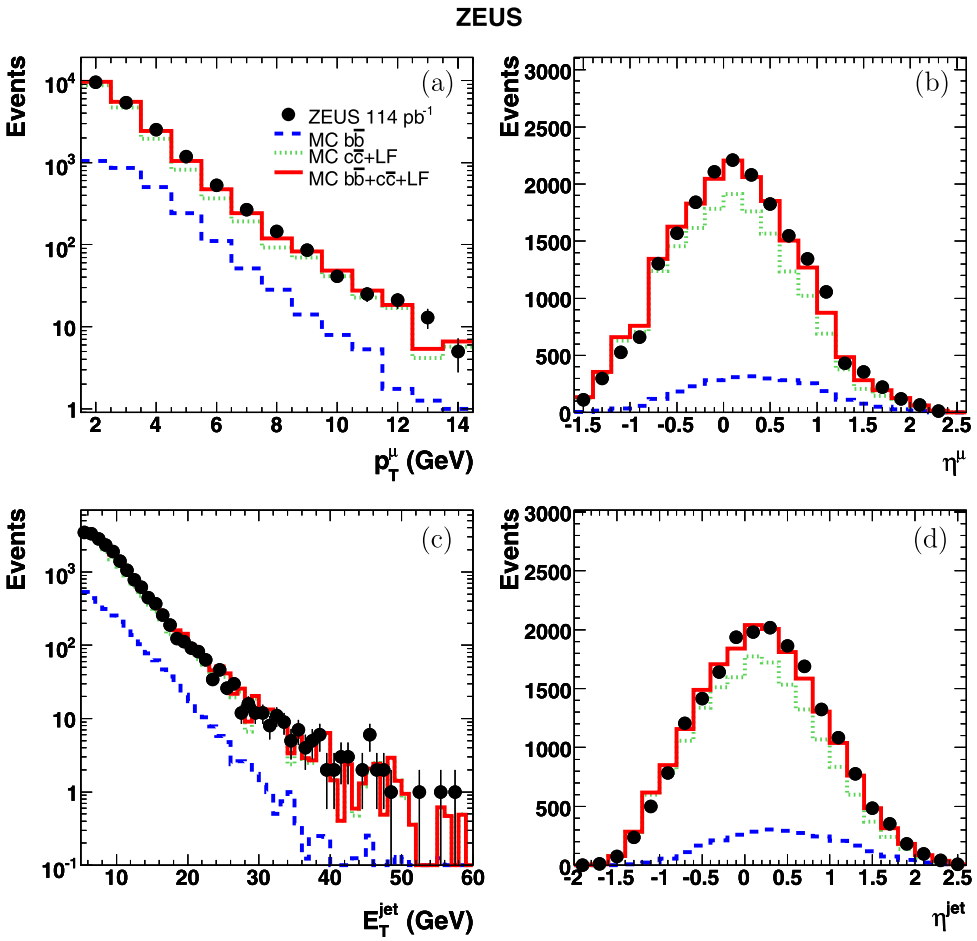

Fig. 1 Data (*dots*) compared to MC predictions (*histograms*) using the p_T^{rel}-fit after final cuts, for which beauty (*dashed*), charm and light flavours (*dotted*) are combined (*continous*) as described in Sect. 6. The distributions of (**a**) p_T^{μ}, (**b**) η^{μ}, (**c**) E_T^{jet} and (**d**) η^{jet} are shown. Only statistical uncertainties are given

in the Breit frame. The parton density functions (PDF) were obtained by repeating the ZEUS-S [71] PDF fit in the FFNS with the quark masses set to the same values as in the HVQDIS calculation.

A model of b fragmentation into weakly decaying hadrons and of the decay of b hadrons into muons was used to calculate muon observables from the partonic results. The hadron momentum was obtained by scaling the quark momentum according to the fragmentation function of Peterson et al. [72] with the parameter $\epsilon = 0.0035$. The semileptonic decay spectrum for beauty hadrons was taken from JETSET [66]. Direct ($b \to \mu$) and indirect ($b \to c(\bar{c}) \to \mu$ and $b \to \tau \to \mu$) b-hadron decays to muons were considered together according to their probabilities. The sum of the branching ratios of direct and indirect decays of b hadrons into muons was fixed to 0.22, as implemented in JETSET.[3]

The NLO QCD predictions were multiplied by hadronisation corrections to obtain jet variables comparable to the ones used in the cross section measurement. These corrections are defined as the ratio of the cross sections obtained by applying the jet finder to the four-momenta of all hadrons and that from applying it to the four-momenta of all partons. They were evaluated using the RAPGAP program; they change the NLO QCD predictions by typically 5% or less.

The uncertainty of the theoretical predictions was evaluated by independently varying μ_R and μ_F by a factor of 2 and 1/2 and m_b between 4.5 and 5.0 GeV. Each of these variations resulted in uncertainties of about 5–10% in the kinematic range of this measurement.

The HVQDIS NLO predictions were also used for the extrapolation of the measured visible cross sections to $F_2^{b\bar{b}}$. For this step, uncertainties on the hadronisation corrections, the branching ratios and the shape variation due to the choice of PDF were also included.

Several other predictions are available for $F_2^{b\bar{b}}$. The predictions by the CTEQ [74] and MSTW [75] groups use NLO calculations based on the general-mass variable-flavour-number scheme (VFNS) with different treatments of the flavour-threshold region [76]. The MSTW prediction is also available in a variant partially including NNLO terms [75]. The NLO prediction of GJR [77] is based on the FFNS. The

[3]The small deviation from the latest PDG values [73] is negligible compared to the quoted uncertainties.

Table 1 PDF schemes and parameters of the calculations described in Sect. 5 and shown in Fig. 5

PDF	Order	Scheme	μ_F^2	μ_R^2	m_b (GeV)	α_s
MSTW08 NLO	α_s^2	VFNS	Q^2		4.75	0.1202
MSTW08 NNLO	appr. α_s^3	VFNS	Q^2		4.75	0.1171
CTEQ6.6 NLO	α_s, α_s^2	VFNS	Q^2	$Q^2+m_b^2$	4.5	0.1180
GJR08 NLO	α_s^2	FFNS	m_b^2		4.2	0.1145
ABKM NNLO	appr. α_s^3	FFNS	$Q^2+4m_b^2$		4.5	0.1129
ZEUS-S+HVQDIS	α_s^2	FFNS	$\frac{1}{4}(Q^2+p_T^2+m_b^2)$		4.75	0.1180

prediction of ABKM [78, 79] is based on a partial NNLO FFNS calculation which is almost complete in the threshold region $Q^2 \approx m_b^2$. Each of these calculations were done using PDFs extracted within the respective scheme. The scales, masses and α_s values used by each prediction are summarised in Table 1.

6 Extraction of beauty signal

The beauty signal was extracted from the distribution of the transverse momentum of the muon with respect to the momentum of the associated jet, p_T^{rel}, defined as

$$p_T^{\mathrm{rel}} = \frac{|\vec{p}^{\,\mu} \times \vec{p}^{\,\mathrm{jet}}|}{|\vec{p}^{\,\mathrm{jet}}|},$$

where $\vec{p}^{\,\mu}$ is the muon and $\vec{p}^{\,\mathrm{jet}}$ the jet momentum vector. The fraction of beauty, $f_{b\bar{b}}$, and background, f_{bkg}, events in the sample was obtained from a two-component fit to the shape of the measured p_T^{rel} distribution, d_μ, with a beauty and a background component:

$$d_\mu = f_{b\bar{b}} d_\mu^{b\bar{b}} + f_{\mathrm{bkg}} d_\mu^{\mathrm{bkg}}, \tag{1}$$

where the p_T^{rel} distribution of beauty, $d_\mu^{b\bar{b}}$, was taken from the RAPGAP MC: $d_\mu^{b\bar{b}} = d_\mu^{b\bar{b},\mathrm{MC}}$. The corresponding distribution for the background, d_μ^{bkg}, was obtained from the sum of the LF, d_μ^{LF}, and the charm, $d_\mu^{c\bar{c}}$, distributions weighted according to the charm and LF cross sections predicted by RAPGAP and ARIADNE, respectively,

$$d_\mu^{\mathrm{bkg}} = r d_\mu^{c\bar{c}} + (1-r) d_\mu^{\mathrm{LF}}, \tag{2}$$

where r is the predicted charm fraction. The distribution d_μ^{LF} was obtained using a sample of measured CTD tracks not identified as muons. These tracks, typically from a π or K meson, were required to fulfill the same momentum and angular cuts as the selected muons; they are called unidentified tracks in the following. The p_T^{rel} distribution for unidentified tracks, d_x, is expected to be similar to d_μ^{LF}, under the assumption that the probability for an unidentified track to be identified as a muon, $P_{x\to\mu}$, does not depend strongly on p_T^{rel}. Monte Carlo predictions for d_μ^{LF} and d_x were used to correct d_x:

$$d_\mu^{\mathrm{LF}} = d_x \frac{d_\mu^{\mathrm{LF,MC}}}{d_x^{\mathrm{MC}}}. \tag{3}$$

The ratio $d_\mu^{\mathrm{LF,MC}}/d_x^{\mathrm{MC}}$ accounts for differences between d_μ^{LF} and d_x due to a residual p_T^{rel} dependence of $P_{x\to\mu}$ and for the charm and beauty contamination in the unidentified track sample.

The data cannot be used to extract the distribution $d_\mu^{c\bar{c}}$. Two different options were therefore considered to describe it: the distribution given by the RAPGAP MC, i.e. $d_\mu^{c\bar{c}} = d_\mu^{c\bar{c},\mathrm{MC}}$, or the same distribution corrected using the unidentified track sample, as in the case of the LF background:

$$d_\mu^{c\bar{c}} = \frac{d_x}{d_x^{\mathrm{MC}}} d_\mu^{c\bar{c},\mathrm{MC}}. \tag{4}$$

The average of these two distributions was taken as the nominal $d_\mu^{c\bar{c}}$. The small differences between them were treated as a systematic uncertainty.

Figure 2 shows the measured distribution of the muon p_T^{rel} together with the results of the fit according to (1). The fitted sum of the two components reproduces the data reasonably well. The fraction of beauty in the total sample is

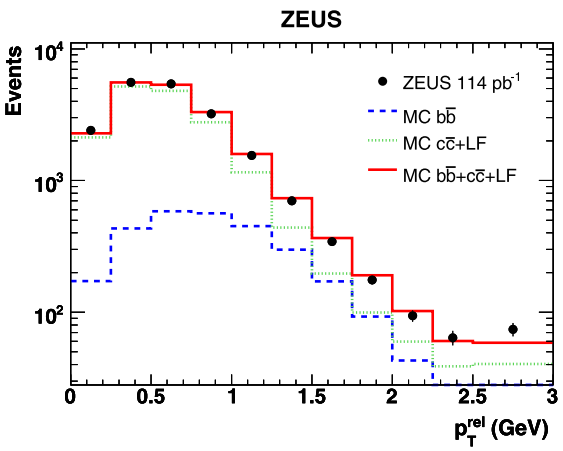

Fig. 2 Measured p_T^{rel}-distribution and fit from MC. Details as in Fig. 1

$f_{b\bar{b}} = 0.16 \pm 0.01$ (stat.). For the determination of differential cross sections, the fraction of beauty events in the data was extracted by a fit performed in each cross-section bin.

The average cross sections obtained from the two different running periods ($\sqrt{s} = 300$ and 318 GeV) are expressed in terms of a single cross section at $\sqrt{s} = 318$ GeV. The correction factor of +2% was obtained using the HVQDIS NLO calculation.

7 Systematic uncertainties

The systematic uncertainties on the measured cross sections were determined by varying the analysis procedure or by changing the selection cuts within the resolution of the respective variable and repeating the extraction of the cross sections. The numbers given below give the uncertainty on the total visible cross section, $\sigma_{b\bar{b}}$. The systematic uncertainties on the differential distributions were determined bin-by-bin, unless stated otherwise. The following systematic studies were carried out:

- muon detection: the differences between cross sections derived from muons identified in the BAC and those found in the muon chambers was used to estimate the effect of the uncertainty in the muon detection. The resulting value of ±7% was used for all bins;
- fit of the beauty fraction: the uncertainty related to the signal extraction was estimated by changing the charm contribution to the background, r, by +20% and −20% in (2). This leads to a systematic uncertainty of $^{+4}_{-3}$%;
- background p_T^{rel} shape uncertainty: the charm p_T^{rel} shape, $d_\mu^{c\bar{c}}$, in (2) was varied between the prediction from RAPGAP and that obtained applying the correction from the unidentified track sample in (4). In addition, the correction functions $1 - \frac{d_\mu^{\mathrm{LF,MC}}}{d_x^{\mathrm{MC}}}$ and $1 - \frac{d_x}{d_x^{\mathrm{MC}}}$ in (3) and (4) were varied by ±50%, resulting in a ±9% cross-section uncertainty;
- charm semi-leptonic decay spectrum: the reweighting to the CLEO model was varied by ±50%, resulting in an uncertainty of ±4%;
- energy scale: the effect of the uncertainty in the absolute CAL energy scale of ±2% for hadrons and of ±1% for electrons was $^{+4}_{-5}$%;
- cut on E_T^{cal}: a change of the cut by ±1 GeV leads to changes in the cross section of $^{+2}_{-1}$%;
- cut on N_{Tracks}: a change of the cut to ≥ 7 or to ≥ 9 leads to an uncertainty of $^{+2}_{-1}$%;
- trigger efficiency: the uncertainty on the trigger efficiency for events with $Q^2 < 20$ GeV^2 was ±2%.

All systematic uncertainties were added in quadrature. In addition, a 2% overall normalisation uncertainty associated with the luminosity measurement was added in quadrature to the uncertainty of the total cross section. This uncertainty was not included for the differential cross sections.

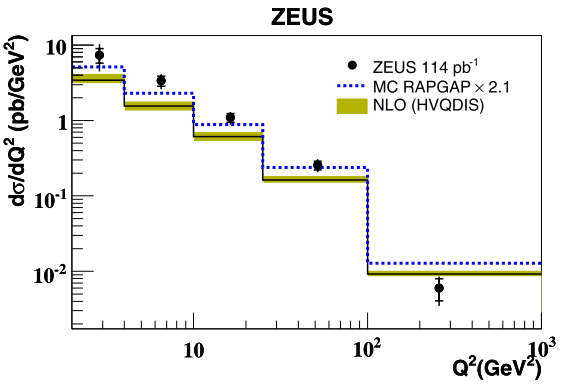

Fig. 3 Differential beauty cross section as a function of the photon virtuality, Q^2, for events with at least one jet and one muon, compared to the RAPGAP LO+PS MC normalised to the data, and compared to the HVQDIS NLO QCD calculations. The errors on the data points correspond to the statistical uncertainty (*inner error bars*) and to the statistical and systematic uncertainty added in quadrature (*outer error bars*). The *shaded bands* show the uncertainty of the theoretical prediction originating from the variation of the renormalisation and factorisation scales and the b-quark mass

8 Cross section

A total visible cross section of

$$\sigma_{b\bar{b}} = 70.4 \pm 5.6\ (\mathrm{stat.}) \pm^{11.4}_{11.3}\ (\mathrm{syst.})\ \mathrm{pb}$$

was measured for the reaction $ep \to eb\bar{b}X \to e\,\mathrm{jet}\,\mu\ X'$ in the kinematic region defined by: $Q^2 > 2\,\mathrm{GeV}^2$, $0.05 < y < 0.7$, and at least one jet with $E_T^{\mathrm{jet}} > 5$ GeV and $-2 < \eta^{\mathrm{jet}} < 2.5$ including a muon of $p_T^\mu > 1.5$ GeV and $\eta^\mu > -1.6$ inside a cone of $\Delta R < 0.7$ to the jet axis. Jets were obtained using the k_T cluster algorithm KTCLUS [62] at the hadron level in its massive mode with the E_T recombination scheme. Weakly decaying B-hadrons were treated as stable particles and were decayed (e.g. to a muon) only after application of the jet algorithm.

This result is to be compared to the HVQDIS NLO prediction of

$$\sigma_{b\bar{b}}^{\mathrm{NLO}} = 46.4 \pm^{5.8}_{6.1}\ \mathrm{pb},$$

where the uncertainty is calculated as described in Sect. 5.

Figure 3 and Table 2 show the differential cross section[4] as a function of Q^2 compared to the HVQDIS NLO calcu-

[4] Cross section integrated over the bin, divided by the bin width.

Table 2 Measured cross sections in bins of Q^2, p_T^μ, η^μ, p_T^{jet} and η^{jet} for beauty production with a muon and a jet as defined in Sect. 8. The statistical and systematic uncertainties are shown separately. The cross sections have an additional global uncertainty of 2% from the luminosity uncertainty. The NLO cross sections and their uncertainties were calculated with HVQDIS

Q^2 bin (GeV^2)	$d\sigma/dQ^2$	δ_{stat} (pb/GeV^2)	δ_{syst}	$d\sigma^{\text{NLO}}/dQ^2$ (pb/GeV^2)
2–4	7.4	±1.6	$^{+2.4}_{-2.4}$	$3.4^{+0.7}_{-0.3}$
4–10	3.38	±0.51	$^{+0.56}_{-0.57}$	$1.56^{+0.21}_{-0.26}$
10–25	1.10	±0.14	$^{+0.14}_{-0.15}$	$0.61^{+0.08}_{-0.10}$
25–100	0.255	±0.033	$^{+0.040}_{-0.036}$	$0.163^{+0.018}_{-0.020}$
100–1000	0.0060	±0.0020	$^{+0.0016}_{-0.0016}$	$0.0092^{+0.0008}_{-0.0011}$
p_T^μ (GeV)	$d\sigma/dp_T^\mu$	δ_{stat} (pb/GeV)	δ_{syst}	$d\sigma^{\text{NLO}}/dp_T^\mu$ (pb/GeV)
1.5–2.5	32.7	±4.4	$^{+6.3}_{-6.0}$	$18.4^{+2.6}_{-3.0}$
2.5–4.0	15.4	±2.2	$^{+2.1}_{-2.0}$	$11.9^{+1.5}_{-1.4}$
4.0–6.0	5.02	±0.90	$^{+0.64}_{-0.60}$	$3.66^{+0.35}_{-0.46}$
6.0–10.0	0.91	±0.29	$^{+0.13}_{-0.14}$	$0.59^{+0.04}_{-0.07}$
η^μ	$d\sigma/d\eta^\mu$	δ_{stat} (pb)	δ_{syst}	$d\sigma^{\text{NLO}}/d\eta^\mu$ (pb)
−1.6– −0.5	8.7	±2.7	$^{+1.3}_{-1.6}$	$5.4^{+0.8}_{-0.5}$
−0.5–0.2	16.2	±4.6	$^{+3.1}_{-3.3}$	$16.7^{+2.3}_{-2.5}$
0.2–0.9	27.9	±3.6	$^{+4.8}_{-4.5}$	$19.0^{+2.1}_{-2.8}$
0.9–2.5	17.1	±1.9	$^{+1.8}_{-1.8}$	$9.4^{+1.2}_{-1.2}$
p_T^{jet} (GeV)	$d\sigma/dp_T^{\text{jet}}$	δ_{stat} (pb/GeV)	δ_{syst}	$d\sigma^{\text{NLO}}/dp_T^{\text{jet}}$ (pb/GeV)
4–10	6.96	±0.75	$^{+1.66}_{-1.52}$	$4.54^{+0.64}_{-0.68}$
10–15	2.69	±0.39	$^{+0.26}_{-0.23}$	$2.37^{+0.29}_{-0.28}$
15–30	0.64	±0.14	$^{+0.09}_{-0.07}$	$0.43^{+0.03}_{-0.05}$
η^{jet}	$d\sigma/d\eta^{\text{jet}}$	δ_{stat} (pb)	δ_{syst}	$d\sigma^{\text{NLO}}/d\eta^{\text{jet}}$ (pb)
−1.6– −0.5	14.4	±3.1	$^{+2.0}_{-2.2}$	$6.2^{+0.9}_{-0.5}$
−0.5–0.2	14.8	±3.8	$^{+2.7}_{-2.8}$	$16.4^{+2.0}_{-2.9}$
0.2–0.9	24.0	±3.8	$^{+4.4}_{-4.4}$	$18.2^{+1.9}_{-2.7}$
0.9–2.5	17.1	±2.2	$^{+2.3}_{-2.2}$	$9.4^{+1.3}_{-1.2}$

lation, and the RAPGAP MC prediction scaled to the data. Differential cross sections as functions of p_T^μ, η^μ, p_T^{jet} and η^{jet} are given in Fig. 4. In shape, both the MC and the NLO QCD calculation reasonably describe the data. The difference in normalisation is correlated to and consistent with the difference observed for the total cross section. The largest fraction of the observed difference of about 2 standard deviations can be attributed to the low x and Q^2, and therefore low p_T, region.

9 Extraction of $F_2^{b\bar{b}}$

The beauty contribution to the proton structure-function F_2, $F_2^{b\bar{b}}$, can be defined in terms of the inclusive double-differential $b\bar{b}$ cross section in Q^2 and x as

$$\frac{d^2\sigma^{b\bar{b}}}{dx\,dQ^2} = \frac{2\pi\alpha^2}{Q^4 x}\left(\left[1+(1-y)^2\right]F_2^{b\bar{b}}\left(x,Q^2\right) - y^2 F_L^{b\bar{b}}\left(x,Q^2\right)\right).$$

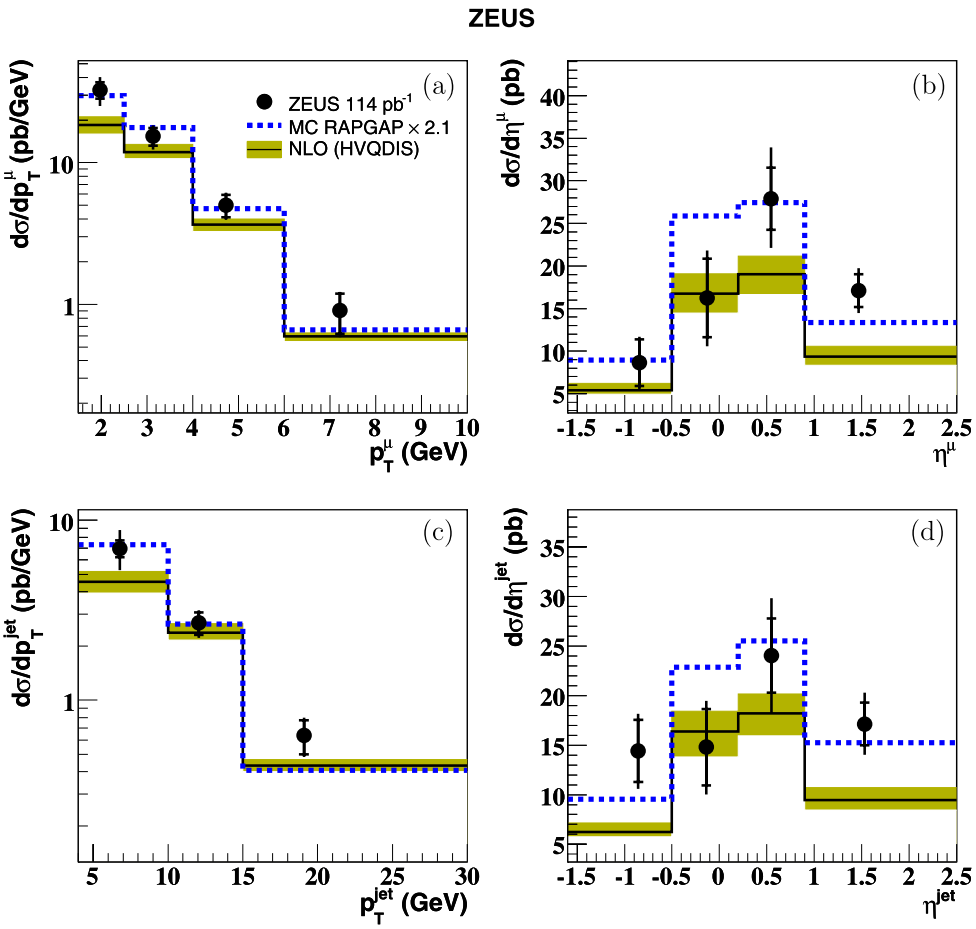

Fig. 4 Differential beauty cross section as a function of (**a**) p_T^{μ}, (**b**) η^{μ}, (**c**) p_T^{jet} and (**d**) η^{jet} compared to the HVQDIS NLO QCD calculations and to the scaled RAPGAP MC. Other details as in Fig. 3

The contribution from F_L is small for the measured Q^2 and x ranges and was neglected. The reduced cross section for events containing b quarks, $\tilde{\sigma}^{b\bar{b}}(x, Q^2) \approx F_2^{b\bar{b}}$, is defined as

$$\tilde{\sigma}^{b\bar{b}}(x, Q^2) = \frac{d^2\sigma^{b\bar{b}}}{dx\, dQ^2} \frac{xQ^4}{2\pi\alpha^2(1+(1-y)^2)}.$$

In this paper, the $b\bar{b}$ cross section is obtained by measuring the process $ep \to eb\bar{b}X \to e\,\text{jet}\,\mu\, X'$. The extrapolation from the measured range to the full kinematic phase space is performed using HVQDIS to calculate $\tilde{\sigma}^{b\bar{b}}_{\text{NLO}}(x, Q^2)$. The reduced cross section is then determined using the ratio of the measured, $\frac{d^2\sigma^{b\bar{b}\to\mu}}{dx\, dQ^2}$, to calculated, $\frac{d^2\sigma^{b\bar{b}\to\mu}_{\text{NLO}}}{dx\, dQ^2}$, double-differential cross sections:

$$\tilde{\sigma}^{b\bar{b}}(x_i, Q_i^2) = \tilde{\sigma}^{b\bar{b}}_{\text{NLO}}(x_i, Q_i^2) \frac{d^2\sigma^{b\bar{b}\to\mu}}{dx\, dQ^2} \Big/ \frac{d^2\sigma^{b\bar{b}\to\mu}_{\text{NLO}}}{dx\, dQ^2}. \quad (5)$$

The measurement was performed in bins of Q^2 and x, see Table 3. The Q^2 and x values for which $F_2^{b\bar{b}}$ was extracted, see Table 4, were chosen close to the centre-of-gravity of each Q^2 and x bin.

Predictions for $F_2^{b\bar{b}}$ were obtained in the FFNS using HVQDIS. In this calculation, the same parton densities, beauty mass and factorisation and renormalisation scales were used as for the NLO predictions for the differential and double-differential cross sections discussed above. The uncertainty of the extrapolation was estimated by varying the settings of the calculation (see Sect. 8) for $\tilde{\sigma}^{b\bar{b}}_{\text{NLO}}(x_i, Q_i^2)$ and $d^2\sigma^{b\bar{b}\to\mu}_{\text{NLO}}/dx\, dQ^2$ and adding the resulting uncertainties in quadrature. The extrapolation uncertainties are listed in Table 4.

The result of the $F_2^{b\bar{b}}$ extraction is shown in Fig. 5, together with values from a previous ZEUS measurement [17] focusing on the higher Q^2 region, and H1 measurements [18–20] using a completely different measurement technique. The HVQDIS + ZEUS-S NLO prediction and other predictions with different parameters (see Sect. 5) are also shown.

The data are all compatible within uncertainties; at low x, the new measurements, in agreement with the previous ZEUS measurement, have a tendency to lie slightly above the H1 data. The largest difference is about 2 standard deviations. The new measurement extends the kinematic coverage down to $Q^2 = 3\ \text{GeV}^2$ and $x = 0.00013$. The predictions from different theoretical approaches agree fairly well with

Table 3 Measured cross sections for different Q^2, x bins for beauty production with a muon and a jet as defined in Sect. 9. For each bin, the Q^2 and $\log_{10} x$ borders are shown. The centre-of-gravity, calculated to NLO using HVQDIS, is given for illustration only. The term $\frac{d\sigma}{d\log_{10} x}$ can also be read as $\frac{1}{x \log 10}\frac{d\sigma}{dx}$. The statistical and systematic uncertainties are shown separately. The cross sections have an additional global uncertainty of 2% from the luminosity uncertainty. The NLO cross sections and their uncertainties were calculated with HVQDIS

Q^2 bin (GeV^2)	$\log_{10} x$ bin	centre-of-gravity Q^2, $\log_{10} x$	$\frac{d^2\sigma^{b\bar{b}\to\mu}}{d\log_{10} x\, dQ^2}$	δ_{stat} ($\mathrm{pb/GeV}^2$)	δ_{syst}	$\frac{d^2\sigma^{b\bar{b}\to\mu}_{\mathrm{NLO}}}{d\log_{10} x\, dQ^2}$ ($\mathrm{pb/GeV}^2$)
2–4	−4.60– −3.50	2.86, −3.98	6.3	±1.5	$\pm^{1.4}_{1.3}$	$2.4\pm^{0.4}_{0.4}$
4–20	−4.40– −3.75	6.12, −3.91	0.83	±0.17	$\pm^{0.14}_{0.13}$	$0.26\pm^{0.05}_{0.04}$
4–20	−3.75– −3.45	8.58, −3.65	2.37	±0.42	$\pm^{0.37}_{0.36}$	$0.83\pm^{0.14}_{0.13}$
4–20	−3.45– −2.50	12.45, −3.12	0.80	±0.15	$\pm^{0.12}_{0.12}$	$0.48\pm^{0.06}_{0.07}$
20–45	−3.60– −3.00	28.78, −3.19	0.587	±0.086	$\pm^{0.067}_{0.073}$	$0.178\pm^{0.020}_{0.031}$
20–45	−3.00– −1.00	32.50, −2.68	0.100	±0.034	$\pm^{0.027}_{0.024}$	$0.079\pm^{0.011}_{0.010}$
45–100	−3.30– −2.60	64.36, −2.82	0.150	±0.033	$\pm^{0.021}_{0.020}$	$0.067\pm^{0.016}_{0.007}$
45–100	−2.60– −1.00	71.74, −2.29	0.045	±0.014	$\pm^{0.011}_{0.009}$	$0.035\pm^{0.003}_{0.004}$
100–250	−3.00– −2.30	145.69, −2.49	0.0206	±0.0089	$\pm^{0.0051}_{0.0067}$	$0.0174\pm^{0.0018}_{0.0014}$
100–250	−2.30– −1.00	168.03, −1.99	0.0054	±0.0056	$\pm^{0.0032}_{0.0024}$	$0.0135\pm^{0.0012}_{0.0012}$
250–3000	−2.50– −1.00	544.53, −1.73	0.00065	±0.00027	$\pm^{0.00013}_{0.00013}$	$0.00071\pm^{0.00004}_{0.00004}$

Table 4 Extracted values of $F_2^{b\bar{b}}$. The statistical and systematic uncertainties are shown separately. The uncertainty of the extrapolation to the full muon and jet phase space of the reaction $ep \to eb\bar{b}X \to e\,\mathrm{jet}\,\mu\; X'$ is also shown. The cross sections have an additional global uncertainty of 2% from the luminosity uncertainty

Q^2 (GeV^2)	x	$F_2^{b\bar{b}}$	δ_{stat}	δ_{syst}	$\delta_{\mathrm{extrapol}}$
3	0.00013	0.0026	±0.0006	$\pm^{0.0012}_{0.0010}$	$\pm^{0.0006}_{0.0003}$
5	0.00013	0.0057	±0.0012	$\pm^{0.0020}_{0.0019}$	$\pm^{0.0005}_{0.0005}$
12	0.0002	0.0138	±0.0024	$\pm^{0.0046}_{0.0048}$	$\pm^{0.0022}_{0.0026}$
12	0.0005	0.0059	±0.0011	$\pm^{0.0022}_{0.0021}$	$\pm^{0.0013}_{0.0011}$
25	0.0005	0.0279	±0.0041	$\pm^{0.0119}_{0.0070}$	$\pm^{0.0099}_{0.0020}$
40	0.002	0.0101	±0.0034	$\pm^{0.0055}_{0.0055}$	$\pm^{0.0005}_{0.0010}$
60	0.002	0.0268	±0.0058	$\pm^{0.0096}_{0.0092}$	$\pm^{0.0031}_{0.0019}$
80	0.005	0.0129	±0.0039	$\pm^{0.0063}_{0.0060}$	$\pm^{0.0008}_{0.0003}$
130	0.002	0.0257	±0.0111	$\pm^{0.0172}_{0.0178}$	$\pm^{0.0029}_{0.0001}$
130	0.005	0.0061	±0.0063	$\pm^{0.0095}_{0.0093}$	$\pm^{0.0003}_{0.0005}$
450	0.013	0.0155	±0.0066	$\pm^{0.0099}_{0.0098}$	$\pm^{0.0013}_{0.0002}$

each other. The HVQDIS predictions are somewhat lower than the ZEUS data at low Q^2 and x, where the influence of the beauty-quark mass is highest, while at higher Q^2 the data are well described by all predictions.

10 Conclusions

The production of beauty quarks in the deep inelastic scattering process $ep \to eb\bar{b}X \to e\,\mathrm{jet}\,\mu\; X'$ has been studied with the ZEUS detector at HERA. Differential cross sections as a function of Q^2, p_T^μ, η^μ, p_T^{jet} and η^{jet} were measured. In all distributions, the data are reasonably described in shape by the Monte Carlo and by the HVQDIS NLO QCD calculation. However, at low Q^2 and transverse momenta, where the mass effect is largest, HVQDIS tends to underestimate the measured values. The extracted values of $F_2^{b\bar{b}}$ extend the kinematic range towards lower Q^2 and x with respect to previous measurements. They are reasonably described

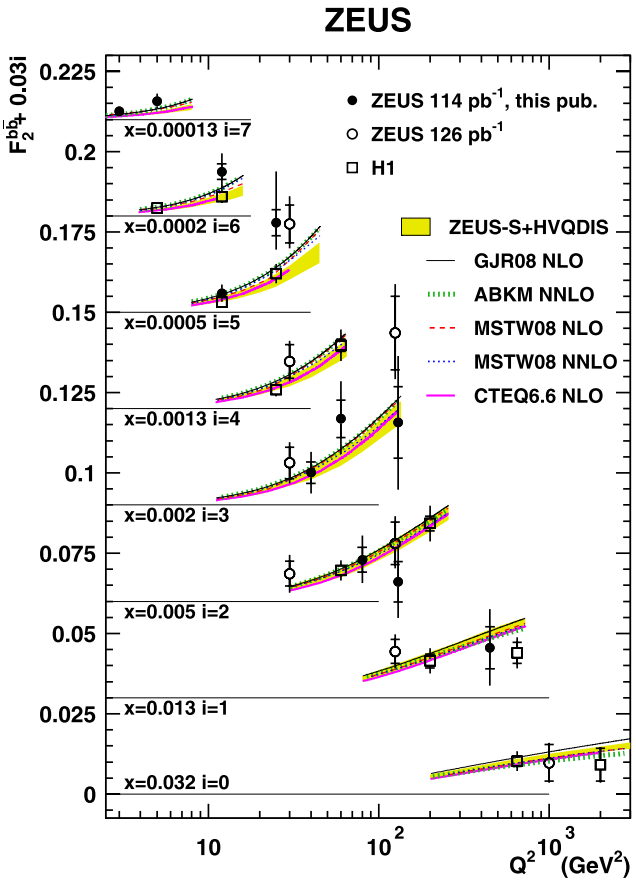

Fig. 5 $F_2^{b\bar{b}}$ as a function of Q^2. The errors on the data points (*filled circles*) correspond to the statistical uncertainty (*inner error bars*) and to the statistical and systematical uncertainty added in quadrature (*outer error bars*). The *horizontal lines* indicate the zero-line for each series of measurements. Results from previous measurements (*open symbols*) and from different QCD predictions (*lines and band*) are also shown. See Sect. 5 and Table 1 for details

by different QCD predictions, whose spread is smaller than the current experimental uncertainty.

Acknowledgements We appreciate the contributions to the construction and maintenance of the ZEUS detector of many people who are not listed as authors. The HERA machine group and the DESY computing staff are especially acknowledged for their success in providing excellent operation of the collider and the data-analysis environment. We thank the DESY directorate for their strong support and encouragement.

References

1. S. Frixione et al., Nucl. Phys. B **412**, 225 (1994)
2. S. Frixione, P. Nason, G. Ridolfi, Nucl. Phys. B **454** (1995)
3. M. Cacciari, S. Frixione, P. Nason, J. High Energy Phys. **0103**, 006 (2001)
4. B.W. Harris, J. Smith, Nucl. Phys. B **452**, 109 (1995)
5. B.W. Harris, J. Smith, Phys. Lett. B **353**, 535 (1995). Erratum-ibid B **359** 423 (1995)
6. B.W. Harris, J. Smith, Phys. Rev. D **57**, 2806 (1998)
7. H1 Coll., C. Adloff et al., Phys. Lett. B **467**, 156 (1999)
8. ZEUS Coll., J. Breitweg et al., Eur. Phys. J. C **18**, 625 (2001)
9. ZEUS Coll., S. Chekanov et al., Phys. Rev. D **70**, 12008 (2004). Erratum-ibid D **74**, 059906 (2006)
10. H1 Coll., A. Aktas et al., Eur. Phys. J. C **41**, 453 (2005)
11. H1 Coll., A. Aktas Eur. Phys. J. C **47**, 597 (2006)
12. ZEUS Coll., S. Chekanov et al., Eur. Phys. J. C **50**, 1434 (2007)
13. ZEUS Coll., S. Chekanov et al., Phys. Rev. D **78**, 072001 (2008)
14. ZEUS Coll., S. Chekanov et al., J. High Energy Phys. **04**, 133 (2009)
15. ZEUS Coll., S. Chekanov et al., J. High Energy Phys. **02**, 032 (2009)
16. ZEUS Coll., S. Chekanov et al., Phys. Lett. B **599**, 173 (2004)
17. ZEUS Coll., S. Chekanov et al., Eur. Phys. J. C **65**, 65 (2009)
18. H1 Coll., A. Aktas et al., Eur. Phys. J. C **40**, 349 (2005)
19. H1 Coll., A. Aktas et al., Eur. Phys. J. C **45**, 23 (2006)
20. H1 Coll., F.D. Aaron et al., Eur. Phys. J. C **65**, 89 (2009)
21. UA1 Coll., C. Albajar et al., Phys. Lett. B **186**, 237 (1987)
22. UA1 Coll., C. Albajar et al., Phys. Lett. B **213**, 405 (1988)
23. UA1 Coll., C. Albajar et al., Phys. Lett. B **256**, 121 (1991). Erratum-ibid. B **262**, 497 (1991)
24. UA1 Coll., C. Albajar et al., Z. Phys. C **61**, 41 (1994)
25. CDF Coll., F. Abe et al., Phys. Rev. Lett. **71**, 500 (1993)
26. CDF Coll., F. Abe et al., Phys. Rev. Lett. **71**, 2396 (1993)
27. CDF Coll., F. Abe et al., Phys. Rev. Lett. **75**, 1451 (1995)
28. CDF Coll., F. Abe et al., Phys. Rev. D **53**, 1051 (1996)
29. CDF Coll., F. Abe et al., Phys. Rev. D **55**, 2546 (1997)
30. CDF Coll., D. Acosta et al., Phys. Rev. D **65**, 052005 (2002)
31. CDF Coll., D. Acosta et al., Phys. Rev. D **66**, 032002 (2002)
32. CDF Coll., D. Acosta et al., Phys. Rev. D **71**, 032001 (2005)
33. CDF Coll., D. Acosta et al., Phys. Rev. D **71**, 092001 (2005)
34. CDF Coll., T. Aaltonen et al., Phys. Rev. D **77**, 072004 (2008)
35. CDF Coll., T. Aaltonen et al., Phys. Rev. D **79**, 092003 (2009)
36. DØColl., S. Abachi et al., Phys. Rev. Lett. **74**, 3548 (1995)
37. DØColl., B. Abbott et al., Phys. Lett. B **487**, 264 (2000)
38. DØColl., B. Abbott et al., Phys. Rev. Lett. **84**, 5478 (2000)
39. DØColl., B. Abbott et al., Phys. Rev. Lett. **85**, 5068 (2000)
40. L3 Coll., M. Acciarri et al., Phys. Lett. B **503**, 10 (2001)
41. L3 Coll., P. Achard et al., Phys. Lett. B **619**, 71 (2005)
42. ALEPH Coll., S. Schael et al., J. High Energy Phys. **0709**, 102 (2007)
43. WA78 Coll., M. Catanesi et al., Phys. Lett. B **202**, 453 (1988)
44. E672/E706 Coll., R. Jesik et al., Phys. Rev. Lett. **74**, 495 (1995)
45. D.M. Jansen et al., Phys. Rev. Lett. **74**, 3118 (1995)
46. E771 Coll., T. Alexopoulos et al., Phys. Rev. Lett. **82**, 41 (1999)
47. HERA-B Coll., I. Abt et al., Eur. Phys. J. C **26**, 345 (2003)
48. ZEUS Coll., U. Holm (ed.), *The ZEUS Detector*. Status Report (unpublished), DESY (1993). Available on http://www-zeus.desy.de/bluebook/bluebook.html
49. N. Harnew et al., Nucl. Instrum. Methods A **279**, 290 (1989)
50. B. Foster et al., Nucl. Phys. Proc. Suppl. B **32**, 181 (1993)
51. B. Foster et al., Nucl. Instrum. Methods A **338**, 254 (1994)
52. M. Derrick et al., Nucl. Instrum. Methods A **309**, 77 (1991)
53. A. Andresen et al., Nucl. Instrum. Methods A **309**, 101 (1991)
54. A. Caldwell et al., Nucl. Instrum. Methods A **321**, 356 (1992)
55. A. Bernstein et al., Nucl. Instrum. Methods A **336**, 23 (1993)
56. G. Abbiendi et al., Nucl. Instrum. Methods A **333**, 342 (1993)
57. T. Jezynski et al., in *Proc. Photonics Applications in Astronomy, Communications, Industry, and High Energy Physics Experiments, SPIE, Vol. 5484*, ed. by R.S. Romaniuk. July 2004 (SPIE, Bellingham, 2004), pp. 180–185
58. J. Andruszków et al., Preprint DESY-92-066, DESY (1992)

59. W.H. Smith, K. Tokushuku, L.W. Wiggers, in *Proc. Computing in High-Energy Physics (CHEP)*, ed. by C. Verkerk, W. Wojcik. Annecy, France, Sept. 1992 (CERN, Geneva, 1992), p. 222. Also in preprint DESY 92-150B
60. F. Jacquet, A. Blondel, in *Proceedings of the Study for an ep Facility for Europe*, ed. by U. Amaldi (Hamburg, Germany, 1979), p. 391. Also in preprint DESY 79/48
61. ZEUS Coll., J. Breitweg et al., Eur. Phys. J. C **1**, 81 (1998)
62. S. Catani, Yu.L. Dokshitzer, B.R. Webber, Phys. Lett. B **285**, 291 (1992)
63. B. Kahle, Ph.D. Thesis, Hamburg University, Hamburg (Germany), Report DESY-THESIS-2006-011 DESY (2006)
64. H. Jung, Comput. Phys. Commun. **86**, 147 (1995)
65. A. Kwiatkowski, H. Spiesberger, H.-J. Möhring, Comput. Phys. Commun. **69**, 155 (1992). [Also in *Proc. Workshop Physics at HERA*, ed. by W. Buchmüller, G. Ingelman (DESY, Hamburg, 1991)]
66. T. Sjöstrand, Comput. Phys. Commun. **82**, 74 (1994)
67. CLEO Coll., N.E. Adam et al., Phys. Rev. Lett. **97**, 251801 (2006)
68. L. Lönnblad, Comput. Phys. Commun. **71**, 15 (1992)
69. R. Brun et al., GEANT3, Technical Report CERN-DD/EE/84-1, CERN (1987)
70. I. Bloch, Ph.D. Thesis, Hamburg University, Hamburg (Germany), Report DESY-THESIS-2005-034, DESY (2005)
71. ZEUS Coll., S. Chekanov et al., Phys. Rev. D **67**, 012007 (2003)
72. C. Peterson et al., Phys. Rev. D **27**, 105 (1983)
73. Particle Data Group, C. Amsler et al., Phys. Lett. B **667**, 1 (2008)
74. CTEQ Coll., P.M. Nadolsky et al., Phys. Rev. D **78**, 013004 (2008)
75. A.D. Martin et al., Eur. Phys. J. C **63**, 189 (2009)
76. R.S. Thorne, W.K. Tung, Preprint arXiv:0809.071 [hep-ph] (2008)
77. M. Glück, P. Jimenez-Delgado, E. Reya, Eur. Phys. J. C **53**, 355 (2008)
78. S. Alekhin et al., Preprint arXiv:0908.2766 [hep-ph] (2009)
79. S. Alekhin, S. Moch, Phys. Lett. B **672**, 166 (2009)